

Hybrid reflections from multiple x-ray scattering in epitaxial bismuth telluride topological insulator films

Sérgio L. Morelhão, Stefan Kycia, Samuel Netzke, Celso I. Fornari, Paulo H. O. Rappl, and Eduardo Abramof

Citation: *Appl. Phys. Lett.* **112**, 101903 (2018); doi: 10.1063/1.5020375

View online: <https://doi.org/10.1063/1.5020375>

View Table of Contents: <http://aip.scitation.org/toc/apl/112/10>

Published by the [American Institute of Physics](#)

Articles you may be interested in

[Unusual negative magnetoresistance in \$\text{Bi}_2\text{Se}_{3-y}\text{S}_y\$ topological insulator under perpendicular magnetic field](#)

Applied Physics Letters **112**, 102401 (2018); 10.1063/1.5019235

[Metamaterials for optical Bragg accelerators](#)

Applied Physics Letters **112**, 101902 (2018); 10.1063/1.5018251

[Rhodium doped InGaAs: A superior ultrafast photoconductor](#)

Applied Physics Letters **112**, 102101 (2018); 10.1063/1.5016282

[Electrical tuning of the band alignment and magnetoconductance in an n-type ferromagnetic semiconductor \(In,Fe\)As-based spin-Esaki diode](#)

Applied Physics Letters **112**, 102402 (2018); 10.1063/1.5010020

[Schottky x-ray detectors based on a bulk \$\beta\text{-Ga}_2\text{O}_3\$ substrate](#)

Applied Physics Letters **112**, 103502 (2018); 10.1063/1.5020178

[Thermally conductive tough flexible elastomers as composite of slide-ring materials and surface modified boron nitride particles via plasma in solution](#)

Applied Physics Letters **112**, 101901 (2018); 10.1063/1.5020325

High Vacuum Performance

The expanded family of TwisTorr FS Turbo Pumps

See the
new pumps



 **Agilent**
Trusted Answers

Hybrid reflections from multiple x-ray scattering in epitaxial bismuth telluride topological insulator films

Sérgio L. Morelhão,^{1,2} Stefan Kycia,¹ Samuel Netzke,¹ Celso I. Fornari,³ Paulo H. O. Rappl,³ and Eduardo Abramof³

¹Department of Physics, University of Guelph, Guelph, Ontario N1G 1W2, Canada

²Institute of Physics, University of São Paulo, São Paulo 05508-090, Brazil

³National Institute for Space Research, São José dos Campos, São Paulo 12227-010, Brazil

(Received 22 December 2017; accepted 21 February 2018; published online 6 March 2018)

Epitaxial films of bismuth telluride topological insulators have received increasing attention due to their potential applications in spintronic and quantum computation. One of the most important properties of epitaxial films is the presence of interface defects due to the lateral lattice mismatch since electrically active defects can drastically compromise device performance. By describing hybrid reflections in hexagonal bismuth telluride films on cubic substrates, in-plane lattice mismatches were characterized with accuracy at least 20 times better than using other X-ray diffraction methods, providing clear evidence of 0.007% lateral lattice mismatch, consistent with stress relaxation associated with van der Waals gaps in the film structure. *Published by AIP Publishing.*

<https://doi.org/10.1063/1.5020375>

Semiconductor and optical industries make broad usage of thin epitaxial films and multilayers. X-ray diffraction (XRD) is an essential tool for the characterization of epitaxial thin films, giving the necessary information about composition, orientation, and structural perfection for both quality control and development of new device technologies. Structure refinement by XRD simulation is the most used approach for accurate data analysis, which is only as reliable as the quality of the best achieved fit of the data. To this purpose, all features (peaks in intensity) in a scan of intensity must be identified.¹ Any disagreement between experimental and simulated data calls into question the actual structure of the thin film.²

Hybrid reflections (HRs) from multiple x-ray diffraction are known to cause extra features in diffraction data of thin films. In general, they can be easily avoided or identified by changing the sample azimuth¹ or they can be used as a tool for studying heteroepitaxial films^{3–7} and superlattices.⁸ In a new class of epitaxial systems with potential applications in spintronic and quantum computation, film and substrate materials have quite different lattices.^{9–12} In these cases, HRs can be nearly inevitable in any scan of intensity. There are no available approaches neither to describe their occurrence nor to use them for analyzing one of the most important properties of epitaxial systems that seriously impact the final performance of the devices, which is the amount of defects due to the lateral lattice mismatch at the film/substrate interface.

Bismuth telluride (Bi₂Te₃) has been recently established as an archetype for three-dimensional topological insulators.^{13,14} Since intrinsic conduction through only topological surface states can be obtained in high-quality thin films,^{10,12} there has been significant investigation on the growth parameters of thin films by molecular beam epitaxy (MBE) where epitaxial films of Bi₂Te₃ with a hexagonal lattice grow along the *c* axis on cubic (111) substrates.^{15–18} van der Waals bonds along the film thickness allow epitaxy on substrates of large lattice mismatch,^{19–23} and the effects of the substrate choice on film quality, surface morphology, and mobility of

charge carriers are also subjects of recent investigations.^{24–26} In this work, we provide a general description of hybrid reflections in such awkward systems, giving the necessary equations to identify and use HRs in the most common XRD methods employed worldwide for studying epitaxial films. Experimentally, we use an in-house x-ray diffractometer to demonstrate and exploit HRs in bismuth telluride films grown by MBE on BaF₂ (111), which has been so far the most suitable substrate for these films due to the very small in-plane lattice mismatch of only 0.04%.^{16,17}

HRs arise from the differences between two distinct crystal lattices that share a common interface. They are produced by sequences of successive $h_s k_s l_s$ reflections in the substrate and $h_f k_f l_f$ reflections in the film, in principle, without any specific order or number of reflections involved on each possible sequence. In reciprocal space, hybrid reflections have diffraction vectors

$$\mathbf{Q}^* = \sum_{f,s} (\mathbf{Q}_f + \mathbf{Q}_s), \quad (1)$$

where \mathbf{Q}_f and \mathbf{Q}_s stand for diffraction vectors on the film and substrate lattices, respectively. In real space, their scattering direction obeys the same rule of any diffraction vector, making an angle

$$\Theta = 2\arcsin(Q^*/Q_{\max}). \quad (2)$$

(usually called 2θ) with the incident x-ray direction, $Q_{\max} = 4\pi/\lambda$ for x-rays of wavelength λ . Regarding the outward normal direction \hat{n} to the common interface, the hybrid diffraction vectors can be decomposed in terms of perpendicular $Q_{\perp}^* = \mathbf{Q}^* \cdot \hat{n}$ and in-plane $Q_{\parallel}^* = \mathbf{Q}^* - Q_{\perp}^* \hat{n}$ components. Then, the x-ray incidence angle at the interface falls within the interval

$$\theta_i = \Theta/2 \pm \arcsin(Q_{\parallel}^*/Q^*) \quad (3)$$

depending on which azimuth \mathbf{Q}^* is excited.

The most relevant fact about HRs is that their occurrence is a direct consequence of differences between both lattices. In other words, when the film and the substrate share identical unit cells and crystallographic orientations, as in homoepitaxy, there will be no extra reciprocal lattice nodes since all \mathbf{Q}^* vectors fall on top of the usual ones from both lattices. Then, the multi-scattering process implied by Eq. (1) simplifies to the well-known multiple diffraction of X-ray in single crystals.^{27,28}

Films coherently strained to their substrates are the simplest systems where HRs can be observed.¹ Along the specular truncation rod, $Q_{\parallel}^* = 0$, $\theta_i = \Theta/2$, and in the scan of intensity versus 2θ , i.e., the typical θ - 2θ scans as usually called, hybrid peaks show up around scattering angles given by Eq. (2) where \mathbf{Q}^* has only the Q_{\perp}^* component, i.e., $\Theta = 2\arcsin(Q_{\perp}^*/Q_{\max})$. It is worthwhile to reemphasize that the observation of hybrid peaks depends on the sample azimuth and the axial divergence of the x-rays plays an important role in observing these peaks. Wider axial divergence results in increased chance of exciting HRs unintentionally.

Formation of interface defects is the typical mechanism by which the elastic stress due to the in-plane lattice mismatch relaxes.^{29,30} When the film is relaxed, the film and the substrate no longer share exactly the same in-plane lattice parameter and $Q_{\parallel}^* \neq 0$ even for the HRs that would be along the specular truncation rod in non-relaxed films. Consequently, a θ - 2θ scan with narrow angular acceptance in 2θ may not even capture those HRs that are slightly off the substrate truncation rods.³¹ Such HRs can be seen by placing the detector at $2\theta = \Theta$, Eq. (2), and carrying out standard rocking curve measurements (scan of intensity versus incidence angle θ), wide enough to satisfy the incidence angle in Eq. (3).

Measuring off-specular-rod HRs as a function of the incidence angle has been the most reliable procedure to evidence a small amount of interface defects in epitaxial films, with accuracy better than the 0.05% limit of standard methods via asymmetric reflections.⁶ Due to the very small mismatch of 0.04%, relaxation of thin Bi_2Te_3 films on BaF_2 (111) is beyond the detectability limit of current methods. Here, a detailed description on how to select suitable HRs to characterize the coherence of film/substrate interfaces is provided, which can also be useful when investigating topological insulator films on substrates of larger lattice mismatch.^{21,26}

Bismuth telluride films have been grown on freshly cleaved (111) BaF_2 substrates using a Riber 32P MBE system that contains a nominal Bi_2Te_3 effusion cell and two extra Te sources.^{17,33} To compensate the loss of tellurium during growth, the ratio Φ_R between the beam equivalent pressures of Te sources and the Bi_2Te_3 effusion cell can be adjusted from $\Phi_R = 0$ (no extra sources of Te) to about $\Phi_R = 6$. Substrate temperature T_S and additional Te impact the deficit of Te in the films.^{16,17} With $T_S = 270^\circ\text{C}$ and $\Phi_R = 3$, a high quality Bi_2Te_3 film with no Te deficit was obtained, while $T_S = 290^\circ\text{C}$ and $\Phi_R = 1$ led to a $\text{Bi}_2\text{Te}_{3-\delta}$ film with significant Te deficit $\delta \simeq 0.4$. Both films were grown for 2 h, at a rate of 0.21 \AA/s , resulting in a thickness of 150 nm. The lateral lattice parameter in bulk materials is known to increase with the deficit of Te, going from 0.4382 nm for $\delta = 0$ to about 0.4409 nm for $\delta = 0.4$,^{16,34} i.e., a variation of 0.6%.

X-ray measurements were carried out using a Huber four circle diffractometer sourced by a fine focus copper rotating anode configured with a double collimating multilayer optics followed by a double bounce Ge 220 channel cut monochromator. The bandwidth is 2 eV for $\text{CuK}\alpha_1$ ($\lambda = 1.540562 \text{ \AA}$). Electronic noise of the point detector is 0.08 counts/s. Adjustment arcs of the goniometer head were used to align the 222_s substrate reflection with the φ rotation axis of the diffractometer with an accuracy better than 0.01° . As reference for sample azimuth, the substrate 313_s and film $01\ 20_f$ asymmetric reflections have been measured in co-planar diffraction geometry at the same azimuth.³³ Hence, the in-plane direction $[110]$ of the film lattice coincides with the $[0\bar{1}1]$ direction of the substrate lattice, and we define $\varphi = 0$ when these directions are in the horizontal diffraction plane pointing upstream. Positive rotation sense of the φ axis is clockwise. The major difference of our x-ray diffractometer regarding commercial ones for thin film analysis is the narrow axial (vertical) divergence of about 0.005° , which is as small as the divergence in the horizontal diffraction plane.

Figures 1(a) and 1(b) show θ - 2θ scans along specular rods of the samples. The $00l_f$ film reflections, labeled L3, L6, ..., L18 ($l_f = 3, 6, \dots, 18$), are clearly visible, as well as the 111_s and 222_s substrate reflections, labeled S1 and S2, respectively. As demonstrated in previous publications,^{16,32} splitting of peaks L3, L6, L12, and L18 in the $\text{Bi}_2\text{Te}_{2.6}$ film [Fig. 1(a)] is caused by the Te deficit that favours bilayers of Bi to form inside the van der Waals gap between two consecutive Bi_2Te_3 quintuple layers (QLs). The Te deficit in this

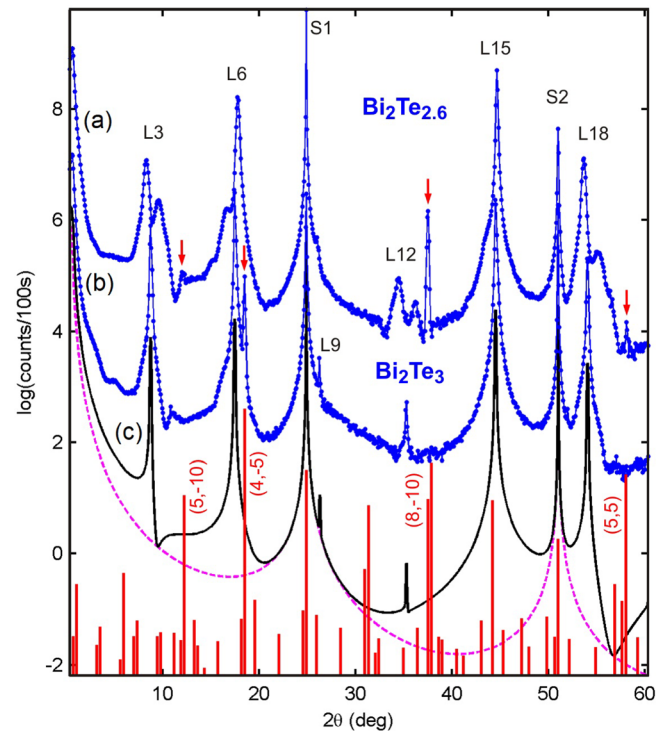


FIG. 1. Long-range θ - 2θ -scans of $\text{Bi}_2\text{Te}_{3-\delta}$ films on BaF_2 (111) substrates. (a) and (b) Experimental scans of films with (a) Te deficit of $\delta = 0.4$ and (b) no Te deficit, $\delta = 0$. (c) Simulated scans of the film/substrate (solid line) and substrate (dashed line).³² L3, L6, ..., L18 are reflections from the film, while S1 and S2 are the 111 and 222 reflections of the substrate. Visible HRs are pointed out by arrows and labeled according to their (n, m) indexes in Eq. (4). Positions of possible HR peaks are indicated by vertical (red) lines.

film means that on average there is one bilayer of Bi for every 6.5 QLs (about 22 bilayers in the whole film thickness). For the second sample, the diffraction pattern in Fig. 1(b) agrees very well with the simulated pattern in Fig. 1(c) for the Bi_2Te_3 film. In both experimental scans, there are several additional peaks (pointed out by arrows), in disagreement with the expected ones for this epitaxial system. These peaks are attributed to HRs.

In the case of this hexagonal-on-cubic growth, the outward normal direction \hat{n} has different representation in each lattice; it stands for the [001] and [111] directions in the film and substrate lattices, respectively. It implies that all HRs have $Q_{\perp}^* = Q^* \cdot \hat{n} = 2\pi(n/a_0\sqrt{3} + m/c)$, and as far as the in-plane mismatch is negligible, HRs along the specular rod have scattering angles

$$\Theta_{nm} = 2\arcsin\left[\frac{\lambda}{2}\left(\frac{n}{a_0\sqrt{3}} + \frac{m}{c}\right)\right], \quad (4)$$

where $n = \sum_s (h_s + k_s + l_s) > 0$ and $m = \sum_f l_f$. By using $a_0 = 6.2001 \text{ \AA}$ as the cubic lattice parameter of BaF_2 and $c = 30.497 \text{ \AA}$ as the hexagonal lattice parameter along the film [001] direction, the 2θ angles of all possible HRs along the specular rod were calculated and compared to experimental ones as shown in Fig. 1; the details about this calculation as well as the relative intensities of the (n, m) families of HRs are given in the [supplementary material](#).

Due to the large value of the c parameter, HRs in this epitaxial system can be found in the seemingly random location in standard θ - 2θ scans. Even in a diffraction system with narrow axial divergence, it is difficult to find an azimuth to perform a θ - 2θ scan without exciting a few HRs, as shown in the θ - 2θ : φ mesh scan in Fig. 2.

Families of (n, m) hybrid peaks follow the threefold axis symmetry of the growth direction. High resolution azimuthal scans of 120° for the two most populated families are shown in Fig. 3. Most hybrid peaks in these scans arise from simple sequences of only two reflections, one in the film and the other in the substrate lattice or vice-versa, i.e., $Q^* = Q_f + Q_s$ or $Q^* = Q_s + Q_f$. Full indexation lists and a script on how to index these hybrids are given in the [supplementary material](#). Here, it is important to identify what are the suitable cases that can be used for studying the in-plane lattice mismatch in these films. Since the in-plane component of the diffraction vectors is easily described in terms of $h_f k_f$ indexes of the $h_f k_f l_f$ reflections of the film hexagonal lattice, a convenient

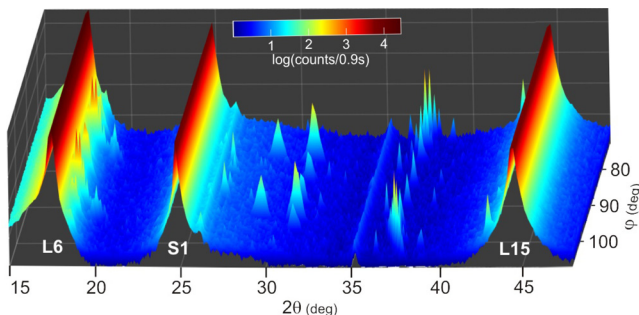


FIG. 2. θ - 2θ : φ mesh scan of $\text{Bi}_2\text{Te}_3/\text{BaF}_2(111)$, revealing some of the main HRs (peaks in φ) of this epitaxial system.

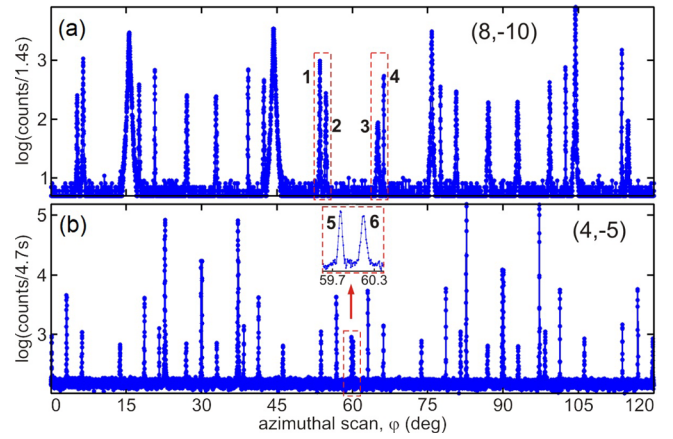


FIG. 3. Azimuthal scans of $\text{Bi}_2\text{Te}_3/\text{BaF}_2$ at fixed incidence angles $\theta_i = \Theta_{nm}/2$, showing two families of (n, m) hybrid peaks. (a) $\theta_i = 18.74^\circ$, hybrids (8, -10), and (b) $\theta_i = 9.24^\circ$, hybrids (4, -5). HRs for characterizing the lateral lattice mismatch are indicated by numbers.

way to write down the in-plane component of Q^* as a function of the in-plane mismatch $\Delta a/a$ is in a first order derivation

$$Q_{\parallel}^* = -Q_{f,\parallel} \Delta a/a, \quad (5)$$

where the in-plane component $Q_{f,\parallel}$ of the film diffraction vector is calculated for $\Delta a/a = 0$.

For a pair of HRs where film and substrate reflections are equivalent but occur on opposite sequences, Q_{\parallel}^* have the same magnitude for both HRs although with opposite signals. If such a pair is excited at the same azimuth within the axial divergence, there will be a split of the observed hybrid peak as a function of the rocking curve angle, i.e., a split regarding the single peak seen for a sample with a coherent strained film. In our diffractometer, the axial divergence is too narrow to excite more than one hybrid at the same

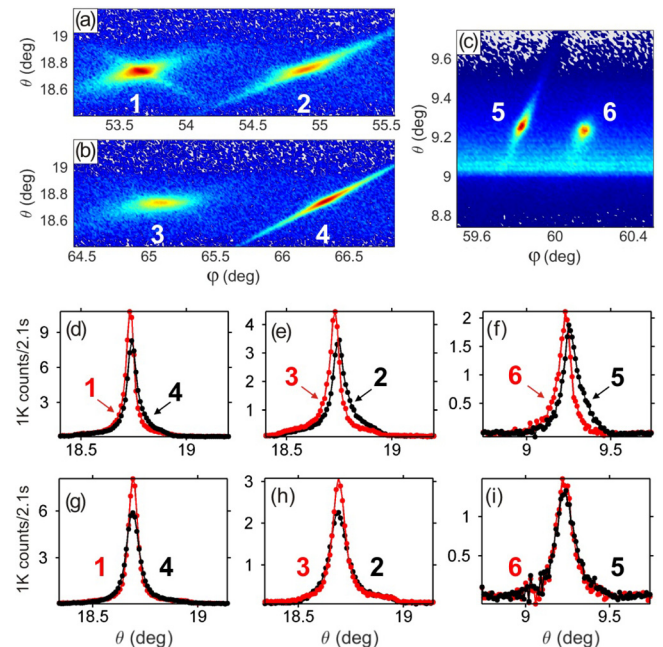


FIG. 4. (a)–(c) Two-dimensional intensity profiles of the hybrid peaks highlighted in Fig. 3. (d)–(i) Intensity of hybrid peaks as a function of the incident angle θ (rocking curves) for the samples with Bi_2Te_3 (d)–(f) and $\text{Bi}_2\text{Te}_{2.6}$ (g)–(i) films.

TABLE I. In-plane mismatch $\Delta a/a$ of Bi_2Te_3 and $\text{Bi}_2\text{Te}_{2.6}$ films on BaF_2 (111), determined by measuring $\Delta\theta_i$ [Eq. (6)] from rocking curves of HR pairs in Figs. 4(d)–4(i).

HR pair	$Q_{f,\parallel}$ (\AA^{-1})	$Q_{f,\parallel} \cdot \hat{k}_{\parallel}/Q^*$	Bi_2Te_3		$\text{Bi}_2\text{Te}_{2.6}$	
			$2\Delta\theta_i$ ($^\circ$)	$2\Delta a/a$ ($\times 10^{-4}$)	$2\Delta\theta_i$ ($^\circ$)	$2\Delta a/a$ ($\times 10^{-4}$)
1 and 4	3.3098	∓ 1.0176	0.0086(35)	$-1.5(6)$	$-0.0019(46)$	$-0.3(8)$
2 and 3	5.9667	± 2.2352	0.0195(43)	$-1.5(3)$	$-0.0025(56)$	$-0.2(4)$
5 and 6	6.6195	± 4.3824	0.0299(58)	$-1.2(3)$	0.0039(88)	0.2(4)

azimuth. Then, we looked up for pairs of nearby hybrid peaks in the azimuthal scans where one of the peaks has a very small width, which in general indicates a hybrid with first reflection occurring in the substrate lattice, and hence a possible pair with opposite sequences of equivalent reflections. The most suitable pairs we found are pointed out by numbers in the azimuthal scans in Fig. 3. Peaks 1 and 4: $22\bar{1}0_f + 044_s$ and $404_s + 02\bar{1}0_f$ are one pair; peaks 2 and 3: $624_s + 14\bar{1}0_f$ and $34\bar{1}0_f + 264_s$ are another pair; and peaks 5 and 6: $444_s + 045_f$ and $445_f + 444_s$ are the only pair where the peaks are less than 1° apart from each other.

To imitate a conventional x-ray diffractometer of wider axial divergence, of about 1° , we perform θ - φ mesh scans around the hybrid peaks pointed out in Fig. 3, and to compare their rocking curves, we integrate the intensity in φ . For the Bi_2Te_3 film, these mesh scans are shown in Figs. 4(a)–4(c), while the rocking curves of each pair are compared in Figs. 4(d)–4(f). For the $\text{Bi}_2\text{Te}_{2.6}$ film, the rocking curves of the same pairs are compared in Figs. 4(g)–4(i). Since hybrids of the (4, -5) family are at the shoulder of reflection 006_f [peak L6 in Fig. 1(b)], the contribution of this reflection has been subtracted from the rocking curves of peaks 5 and 6 in Figs. 4(f)–4(i).

It is interesting to note that the Bi_2Te_3 film is indeed relaxed, as expected in van der Waals epitaxy,²² while the $\text{Bi}_2\text{Te}_{2.6}$ film is perfectly matched to the substrate. The actual shift of hybrid peaks due to film relaxation is estimated from Eqs. (3) and (5) by taking \hat{k}_{\parallel} as the in-plane direction of the incident wavevector \mathbf{k} at the azimuth in which the hybrid is excited. Then, the shift in the rocking curve angle of hybrid peaks as a function of lateral lattice mismatch is given by

$$\Delta\theta_i \simeq -\frac{Q_{f,\parallel} \cdot \hat{k}_{\parallel}}{Q^*} \frac{\Delta a}{a}. \quad (6)$$

From the diffraction geometry of a single reflection, it is straightforward to conclude that $Q_{f,\parallel} \cdot \hat{k}_{\parallel} < 0$ for all hybrids in which the first reflection takes place in the film, i.e., hybrids with diffraction vector $Q^* = Q_f + Q_s$. Relaxation of the film implies $\Delta a/a = (a_{f,\parallel} - a_{s,\parallel})/a_{s,\parallel} < 0$ when considering bulk values where $a_{f,\parallel} < a_{s,\parallel} = a_0/\sqrt{2} = 4.3841 \text{ \AA}$. Therefore, in the case of relaxation of the film, those hybrids with first reflection in the film such as hybrids 1, 3, and 6 shift towards smaller values of the incidence angle, $\Delta\theta_i < 0$ in Eq. (6), while hybrids 2, 4, and 5 shift towards higher angles, $\Delta\theta_i > 0$, exactly as observed in the rocking curves in Figs. 4(d)–4(f).

The values of peak shifting shown in Table I for the Bi_2Te_3 film indicate a mismatch of $\Delta a/a = -7(\pm 2) \times 10^{-5}$,

about 0.007%, while for the $\text{Bi}_2\text{Te}_{2.6}$ film, no mismatch could be detected. The variation in the lattice mismatch due to fluctuation of room temperature is of the order of $1.1 \times 10^{-6}/\text{K}$. For the measured HR pairs with x-rays of 8 keV, refraction corrections³⁵ at the film/substrate interface can account for splitting the hybrid peaks by less than 0.0032° (see [supplementary material](#)), which is smaller than our accuracy in measuring the split of rocking curve peaks. Therefore, misfits of 0.002% in lateral lattice parameters are close to the minimum that can be detected by measuring HR pairs in this epitaxial system without extra protocols for temperature control better than a few degrees and corrections due to refraction. It is comparable to the most accurate methods available for lattice parameter determination in single crystals.^{36,37}

In summary, by using a high resolution method for measuring the lateral lattice mismatch in epitaxial films, we have demonstrated that strain in the film lattice is easily relaxed through van der Waals gaps between monoatomic layers stacking along the growth direction, in spite of the very small mismatch. This is an important mechanism of elastic stress relaxation that can be harmless to device performance since the electric field around van der Waals bonds is much smaller than that around covalent or ionic chemical bonds. In the film with Te deficit, one bilayer of bismuth in the van der Waals gap of every 6 or 7 quintuple layers of Bi_2Te_3 is capable of increasing van der Waals forces, stiffening the structure, and preventing the relaxation of the film. Otherwise, this film would relax to a larger lateral lattice parameter, of about 0.6%, regarding the film without bilayers of bismuth.

See [supplementary material](#) for the choice of reference frame, indexing of hybrid reflections, and corrections due to refraction.

The authors acknowledge the financial support of CAPES (Grant No. 88881.119076/2016-01), FAPESP (Grant No. 2016/22366-5), and Natural Sciences and Engineering Research Council of Canada (NSERC).

¹E. H. Smith, P. D. C. King, A. Soukiassian, D. G. Ast, and D. G. Schlom, *Appl. Phys. Lett.* **111**, 131903 (2017).

²S. L. Morelhão, G. E. S. Brito, and E. Abramof, *Appl. Phys. Lett.* **80**, 407 (2002).

³B. J. Isherwood, B. R. Brown, and M. A. G. Halliwell, *J. Cryst. Growth* **54**, 449 (1981).

⁴S. L. Morelhão and L. P. Cardoso, *J. Appl. Phys.* **73**, 4218 (1993).

⁵S. L. Morelhão and L. P. Cardoso, *Solid State Commun.* **88**, 465 (1993).

⁶J. Z. Domagała, S. L. Morelhão, M. Sarzyński, M. Maździarz, P. Dłużewski, and M. Leszczyński, *J. Appl. Cryst.* **49**, 798 (2016).

⁷Y.-Z. Zheng, Y.-L. Soo, and S.-L. Chang, *Sci. Rep.* **6**, 25580 (2016).

- ⁸S. L. Morelhão, L. H. Avanci, A. A. Quivy, and E. Abramof, *J. Appl. Cryst.* **35**, 69 (2002).
- ⁹P. Cheng, C. Song, T. Zhang, Y. Zhang, Y. Wang, J.-F. Jia, J. Wang, Y. Wang, B.-F. Zhu, X. Chen *et al.*, *Phys. Rev. Lett.* **105**, 076801 (2010).
- ¹⁰G. Wang, X.-G. Zhu, Y.-Y. Sun, Y.-Y. Li, T. Zhang, J. Wen, X. Chen, K. He, L.-L. Wang, X.-C. Ma *et al.*, *Adv. Mater.* **23**, 2929 (2011).
- ¹¹J. J. Lee, F. T. Schmitt, R. G. Moore, I. M. Vishik, Y. Ma, and Z. X. Shen, *Appl. Phys. Lett.* **101**, 013118 (2012).
- ¹²K. Hoefler, C. Becker, D. Rata, J. Swanson, P. Thalmeier, and L. H. Tjeng, *Proc. Natl. Acad. Sci. U.S.A.* **111**, 14979 (2014).
- ¹³H. Zhang, C.-X. Liu, X.-L. Qi, X. Dai, Z. Fang, and S.-C. Zhang, *Nat. Phys.* **5**, 438 (2009).
- ¹⁴Y. L. Chen, J. G. Analytis, J.-H. Chu, Z. K. Liu, S.-K. Mo, X. L. Qi, H. J. Zhang, D. H. Lu, X. Dai, Z. Fang *et al.*, *Science* **325**, 178 (2009).
- ¹⁵Y.-Y. Li, G. Wang, X.-G. Zhu, M.-H. Liu, C. Ye, X. Chen, Y.-Y. Wang, K. He, L.-L. Wang, X.-C. Ma *et al.*, *Adv. Mater.* **22**, 4002 (2010).
- ¹⁶H. Steiner, V. Volobuev, O. Caha, G. Bauer, G. Springholz, and V. Holý, *J. Appl. Cryst.* **47**, 1889 (2014).
- ¹⁷C. I. Fornari, P. H. O. Rappl, S. L. Morelhão, and E. Abramof, *J. Appl. Phys.* **119**, 165303 (2016).
- ¹⁸F. Bonell, M. G. Cuxart, K. Song, R. Robles, P. Ordejón, S. Roche, A. Mugarza, and S. O. Valenzuela, *Cryst. Growth Des.* **17**, 4655 (2017).
- ¹⁹A. Koma, *J. Cryst. Growth* **201-202**, 236 (1999).
- ²⁰Y. Guo, Z. Liu, and H. Peng, *Small* **11**, 3290 (2015).
- ²¹L. He, X. Kou, and K. L. Wang, *Phys. Status Solidi RRL* **7**, 50 (2013).
- ²²A. Ghasemi, D. Kepaptsoglou, P. L. Galindo, Q. M. Ramasse, T. Hesjedal, and V. K. Lazarov, *NPG Asia Mater.* **9**, e402 (2017).
- ²³A. J. Littlejohn, Y. Xiang, E. Rauch, T.-M. Lu, and G.-C. Wang, *J. Appl. Phys.* **122**, 185305 (2017).
- ²⁴J. Kampmeier, S. Borisova, L. Plucinski, M. Luysberg, G. Mussler, and D. Grützmacher, *Cryst. Growth Des.* **15**, 390 (2015).
- ²⁵T. P. Ginley, Y. Wang, and S. Law, *Crystals* **6**, 154 (2016).
- ²⁶Y. Wang, T. P. Ginley, and S. Law, *J. Vac. Sci. Technol. B* **36**, 02D101 (2018).
- ²⁷S.-L. Chang, *X-Ray Multiple-Wave Diffraction: Theory and Application* (Springer-Verlag, Berlin, Heidelberg, 2010).
- ²⁸S. L. Morelhão and S. Kycia, *Phys. Rev. Lett.* **89**, 015501 (2002).
- ²⁹T. Tanabe, S. Zhao, Y. Sato, and Y. Oyama, *J. Appl. Phys.* **122**, 165105 (2017).
- ³⁰L. Yao, S. Inkinen, O. Pacherova, M. Jelinek, S. van Dijken, and M. Tyunina, *Phys. Chem. Chem. Phys.* **6**, 4263 (2018).
- ³¹S. L. Morelhão and J. Z. Domagała, *J. Appl. Cryst.* **40**, 546 (2007).
- ³²S. L. Morelhão, C. I. Fornari, P. H. O. Rappl, and E. Abramof, *J. Appl. Cryst.* **50**, 399 (2017).
- ³³C. I. Fornari, P. H. O. Rappl, S. L. Morelhão, T. R. F. Peixoto, H. Bentmann, F. Reinert, and E. Abramof, *APL Mater.* **4**, 106107 (2016).
- ³⁴H. Lind, S. Lidin, and U. Häussermann, *Phys. Rev. B* **72**, 184101 (2005).
- ³⁵S. L. Morelhão, *Computer Simulation Tools for X-Ray Analysis* (Springer International Publishing, 2016).
- ³⁶W. L. Bond, *Acta Cryst.* **13**, 814 (1960).
- ³⁷J. A. Quilliam, S. Meng, H. A. Craig, L. R. Corruccini, G. Balakrishnan, O. A. Petrenko, A. Gomez, S. W. Kycia, M. J. P. Gingras, and J. B. Kycia, *Phys. Rev. B* **87**, 174421 (2013).